Hydrothermal Synthesis, Structure, and Sorption Properties of the New Microporous Ferric Molybdenum Phosphates $[(CH_3)_4N]_2(NH_4)_2[Fe_2Mo_{12}O_{30}(H_2PO_4)_6(HPO_4)_2]\cdot nH_2O$ and $[(CH_3)_4N]_2Na_4[Fe_3Mo_{12}O_{30}(H_xPO_4)_8]\cdot nH_2O$†

Linda A. Meyer and Robert C. Haushalter*

NEC Research Institute, 4 Independence Way, Princeton, New Jersey 08540

Received June 1, 1992

The first microporous solids incorporating two octahedrally coordinated transition elements, the phosphates $(TMA)_2(NH_4)_2[Fe_2Mo_{12}O_{30}(H_2PO_4)_6(HPO_4)_2]\cdot 11H_2O$ (**1**) and $(TMA)_2Na_4[Fe_3Mo_{12}O_{30}(H_xPO_4)_8]\cdot 16H_2O$ (**2**) (TMA = $(CH_3)_4N^+$), have been hydrothermally synthesized and characterized by single-crystal X-ray diffraction and water absorption isotherms. Phosphate **1** is prepared in 94% yield from Na_2MoO_4, Mo, $FeCl_3$, $(NH_4)_2HPO_4$, (TMA)OH, H_3PO_4, and H_2O in a mole ratio of 5:1:1:2:7:16:150 at 200 °C for 64 h, while **2** is synthesized in 62% yield by the reaction of Na_2MoO_4, Mo, $FeCl_3$, (TMA)OH, H_3PO_4 and H_2O in a mole ratio of 5:1:1:8:18:250 at 200 °C for 3 days. Orange crystals of **1** are rhombohedral, space group $R\bar{3}m$, with a = 14.274(3) Å and α = 51.637(3)° (rhombohedral setting) and V = 1652(1) Å^3, while orange crystals of **2** are triclinic, space group $P\bar{1}$, with a = 12.719(5) Å, b = 13.844(7) Å, c = 12.701(6) Å, α = 109.34(4)°, β = 119.22(3)°, γ = 83.42(5)°, V = 1839(3) Å^3, and Z = 2. Both structures are based on $Fe[Mo_6O_{15}(H_xPO_4)_4]_2$ units which are connected via their phosphate groups to additional Fe^{3+} ions to give three-dimensional frameworks. Both compounds display structures that can be rationalized on the basis of regions of hydrophobic and hydrophilic interactions. The interconnected voids and channels in the ferric molybdenum phosphate frameworks are filled with a mixture of charge-compensating cations and water of solvation. Reversible water absorption isotherms indicate that both compounds are microporous with internal void volumes of about 15 and 25 vol % for **1** and **2**, respectively.

The number of structurally complex solid-state inorganic materials known at present does not rival those of the most complicated organic systems. This is partly due to the relatively small effort expended in the solid-state sciences relative to organic and biological chemistry, but the almost total lack of coherent synthetic methodology is also an important factor. Although extremely complicated inorganic structures can be prepared at high temperatures, as best evidenced by the staggering complexity of certain intermetallic phases,[1,2] hydrothermal synthesis[3] has proven to be an excellent low-temperature synthetic approach to novel solid-state materials. Examples include many naturally occurring solids from the mineral world[4] as well as synthetic materials such as certain zeolites[5] and aluminophosphates.[6] Hydrothermal syntheses share advantages from both high-temperature solid-state synthesis and solution-phase synthesis. One can use solids that are insoluble under ambient conditions as starting materials while achieving the advantages of relatively mild reaction conditions and the ability to obtain the highly crystalline products normally associated with syntheses in fluid phases. The low temperatures also allow the use of thermally less stable organic materials and solvents as "stuffing" to allow a particular framework to crystallize.

The hydrothermal syntheses of many of these complex oxides, such as zeolites[5] and aluminophosphates,[6] take place in the presence of a templating agent around which the framework crystallizes. We have recently used cation-directed hydrothermal techniques, as well as traditional high-temperature solid-state syntheses, to prepare a new class of octahedral–tetrahedral solids based on anionic molybdenum phosphate frameworks.[7] The possibility of using materials such as these molybdenum phosphates, which could possess size- and shape-discriminatory access to an internal micropore volume containing d-block elements, was also discussed. These molybdenum phosphates have been prepared with dimensionalities ranging from molecular entities to covalent three-dimensional (3-D) frameworks. Examples of quasi-molecular ionic aggregates include the large $[Na_{12}(H_3PO_4)\{Mo_6O_{15}(HPO_4)(H_2PO_4)_3\}_4]^{8-}$ units found in $(Et_4N)_6Na_2[Na_{12}(H_3PO_4)\{Mo_6O_{15}(HPO_4)(H_2PO_4)_3\}_4]\cdot xH_2O$[8] as well as $[Na_8In_4(H_2O)_4(H_3PO_4)\{Mo_6O_{15}(HPO_4)(H_2PO_4)_3\}_4]$ clusters.[9] Covalently bonded 1-D polymers were characterized in the material $(Et_4N)_2[Mo_4O_8(PO_4)_{2/2}(H_{1.5}PO_4)_2]\cdot 2H_2O$[10] while an ionic 1-D polymer was found in the sodium-bridged compound $(PPh_4)_2[(H_3O)_2NaMo_6O_{15}(HPO_4)(H_2PO_4)_3]$.[11] Several 2-D layered molybdenum phosphates[12] have been structurally characterized, including those prepared at high temperatures, like $Cs_2Mo_4P_6O_{26}$,[13] as well as hydrothermally synthesized materials

† Some of the early work in this study was performed at the Exxon Research and Engineering Co.

(1) Villars, P.; Calvert, L. D. *Pearson's Handbook of Crystallographic Data for Intermetallic Phases*; American Society for Metals: Metals Park, OH, 1986.
(2) Nesper, R. *Angew. Chem., Int. Ed. Engl.* **1991**, *30*, 789.
(3) Rabenau, A. *Angew. Chem., Int. Ed. Engl.* **1985**, *24*, 1026.
(4) Moore, P. B.; Shen, J. *Nature* **1983**, *306*, 356. A table listing properties and references for 32 naturally occurring zeolites is given in: Szostak, R. *Molecular Sieves Principles of Synthesis and Identification*; Van Nostrand Reinhold: New York, 1989. Schmetzer, K.; Nuber, B.; Tremmel, G. *Neues Jahrb. Mineral., Monatsh.* **1984**, 393.
(5) Occelli, M. L.; Robson, H. E. *Zeolite Synthesis*; American Chemical Society: Washington, DC., 1989. Breck, D. W. *Zeolite Molecular Sieves*; Krieger: Malabar, FL, 1974. Vaughan, D. E. W. In *ZEOLITES: Facts, Figures, Future*; Jacobs, P. A., van Santen, R. A., Eds.; Elsevier: Amsterdam, 1989; pp 95–116. Meier, W. M.; Olson, D. H. *Atlas of Zeolite Structure Types*; Butterworths: London, 1987. Barrer, R. M. *Hydrothermal Chemistry of Zeolites*; Academic Press: New York, 1982.
(6) Szostak, R. *Molecular Sieves Principles of Synthesis and Identification*; Van Nostrand Reinhold: New York, 1989. Meier, W. M.; Olson, D. H. *Atlas of Zeolite Structure Types*; Buttersworth: London, 1987. Occelli, M. L.; Robson, H. E. *Zeolite Synthesis*; American Chemical Society: Washington, DC, 1989; Chapter 23.
(7) Haushalter, R. C.; Mundi, L. A. *Chem. Mater.* **1992**, *4*, 31.
(8) Haushalter, R. C.; Lai, F. W. *Angew. Chem., Int. Ed. Engl.* **1989**, *28*, 743.
(9) Haushalter, R. C.; Mundi, L. A. Unpublished results.
(10) Haushalter, R.; Mundi, L. *J. Am. Chem. Soc.* **1991**, *113*, 6340.
(11) Haushalter, R. C.; Lai, F. W. *Inorg. Chem.* **1989**, *28*, 2904.
(12) Mundi, L. A.; Haushalter, R. C. In *Synthesis, Characterization and Novel Applications of Molecular Sieve Materials*; Maroni, V., Ed.; Materials Research Society: Pittsburgh, PA, 1991.
(13) Lii, K. H.; Haushalter, R. C. *J. Solid State Chem.* **1987**, *69*, 320.

0020-1669/93/1332-1579$04.00/0

like $Na_3[Mo_2O_4(HPO_4)(PO_4)]\cdot 2H_2O$,[14] which displayed interesting ionic conductivity with contributions from both protons and sodium ions.[15] Two-dimensional sheets based on $[Mo_4O_8(PO_4)_{4/2}]^{2-}$ building blocks have been structurally characterized, including those with planar layers like $Pr_4N(NH_4)[Mo_4O_8(PO_4)_2]$[16] and $(Et_2NH_2)_2[Mo_4O_8(PO_4)_2]$[12] and those with ruffled layers like (4-phenylpyridine)$_2[Mo_4O_8(PO_4)_2]$.[12] However the largest number of structurally characterized molybdenum phosphates are found in the covalently bonded 3-D framework materials. There are many examples prepared at high temperatures[7] as well as several hydrothermally synthesized solids. These latter materials[17-21] constitute the first large class of microporous octahedral–tetrahedral framework solids that have been fully characterized by both single-crystal X-ray structures and reversible absorption isotherms and display internal void volumes in the range of 15 to nearly 40 vol %.

To understand how the properties of these complex oxides are related to their structures, a reasonable number of examples have to be synthesized and structurally characterized. In order to explore the hydrothermal incorporation of many different cationic sites, or more than one d-block element, into an oxide framework, we have begun to search for synthetic routes to integrate additional covalently bonded cations into molybdenum phosphate frameworks. These efforts have already yielded metal molybdenum phosphate solids with one-, two-, and three-dimensional structures. In addition to the 3-D framework materials discussed here, we have found 1-D ferric molybdenum phosphate polymers[9] and a zinc molybdenum phosphate[22] with an infinite 2-D sheet structure.

In this paper, we discuss the hydrothermal synthesis, single-crystal X-ray structures, and sorption properties of the ferric molybdenum phosphates $(TMA)_2Na_4[Fe_3Mo_{12}O_{30}(H_2PO_4)_6(HPO_4)_2]\cdot nH_2O$ (**1**) and $(TMA)_2(NH_4)_2[Fe_2Mo_{12}O_{30}(H_xPO_4)_8]\cdot nH_2O$ (**2**), where TMA = $(CH_3)_4N$.

Experimental Section

The compounds were prepared in polytetrafluoroethylene-lined stainless steel containers under autogenous pressure. The Mo metal was less than 2 μm in particle size to achieve convenient reaction rates. The yields are based on Mo used.

$(TMA)_2(NH_4)_2[Fe_2Mo_{12}O_{30}(H_2PO_4)_6(HPO_4)_2]\cdot nH_2O$ (1). The reaction of Na_2MoO_4, Mo, $FeCl_3$, $(NH_4)_2HPO_4$, (TMA)OH, H_3PO_4, and H_2O in a mole ratio of 5:1:1:2:7:16:150 at 200 °C for 64 h gave a 94% yield of **1** based on Mo as orange-red crystals, which were isolated by filtration and washing with water.

$(TMA)_2Na_4[Fe_3Mo_{12}O_{30}(H_xPO_4)_6(HPO_4)_2]\cdot nH_2O$ (2). The reaction of Na_2MoO_4, Mo, $FeCl_3$, (TMA)OH, H_3PO_4, and H_2O in a mole ratio of 5:1:1:8:18:250 at 200 °C for 3 days gave orange-red crystals of **2** in 62% yield based on Mo.

Both **1** and **2** contained a single crystalline phase as judged by comparison of their powder X-ray diffraction patterns with the patterns calculated from the atomic positions derived from the single-crystal structure determinations. The amount of solvent water was determined from thermogravimetric analysis and water absorption isotherms.

The water absorption isotherms were determined for samples brought to constant weight at 100–125 °C and ca. 10^{-3} Torr. The weight change as a function of water vapor pressure was then measured at room temperature. The weight was recorded after the sample remained at constant weight for 15 min.

Table I. Crystallographic Data for **1** and **2**

	1	**2**
empirical formula	$Mo_{12}P_8O_{62}Fe_2N_{15}C_8H_{12}$	$Mo_6F_{1.5}P_4Na_2O_{39}NC_4H_{12}$
fw	2821.01	1527.41
crystal system	rhombohedral	triclinic
lattice params		
a, Å	14.274(3)	12.719(15)
b, Å		13.844(7)
c, Å		12.701(6)
α, deg	51.637(3)	109.34(4)
β, deg		119.22(3)
γ, deg		83.42(5)
V, Å^3	1652(1)	1839(3)
T, °C	20	20
space grup	$R\bar{3}m$ (No. 166)	$P\bar{1}$ (No. 2)
Z	1	2
ρ_{calc}, g/cm^3	2.836	2.759
$\mu_{Cu\ K\alpha}$, cm^{-1}	24.96	28.25
residuals:[a] R (R_w)	0.090 (0.088)	0.065 (0.069)

[a] $R = \sum||F_o| - |F_c||/\sum|F_o|$. $R_w = [\sum w(|F_o| - |F_c|)^2/\sum wF_o^2]^{1/2}$.

The experimental crystallographic data are collected in Table I, the fractional coordinates in Table II, and selected bond distances in Table III.

Results and Discussion

Perhaps the most interesting aspect of this study is the fact that such structurally complex solids as these ferric molybdenum phosphates can be synthesized in high yield from a complicated mixture of simple starting materials. However, a good understanding of the factors influencing the nucleation and crystal growth from the hydrothermal reaction medium is complicated by the large number of independent variables in the synthesis. In addition to the mole ratio of the six or seven reactants in this system, factors such as pH, time, temperature, relative solubilities of the reactants, etc. must also play a role in determining which species is ultimately formed. Fortunately, in the case of the molybdenum phosphates[7] not only are the products often single phase, but they actually form large crystals in relatively high yields.

The synthesis of the ferric molybdenum phosphates **1** and **2** is similar to several known molybdenum phosphate preparations[7] but with the addition of the transition metal halide to the reaction mixture containing the cationic template, molybdenum source, phosphoric acid, and water. The synthesis of **1** and **2** also illustrates how sensitve the outcome of these hydrothermal preparations is to the type and number of the cationic templates. For example, in a typical hydrothermal molybdenum phosphate synthesis (MoO_3 or M_2MoO_4, Mo, H_3PO_4, and H_2O) with TMA^+ present, the presence or absence of additional cations greatly influences which product is obtained. A quantitative yield of $(Me_4N)_{1.3}(H_3O)_{0.7}[Mo_4O_8)PO_4)_2]\cdot 2H_2O$[17] is obtained when no template in addition to TMA^+ is used, the presence of Zn^{2+} gives the zinc molybdenum phosphate $(TMA)_2(H_3O)[Zn_3Mo_6O_{15}(HPO_4)(H_2PO_4)_3]\cdot 11.5\ H_2O$,[22] while in the presence of Fe^{3+}, compounds **1** and **2** are obtained when NH_4^+ and Na^+, respectively, are also in the reaction mixture. We have also isolated a 1-D iron molybdenum phosphate with TMA^+ as one of the cations.[9]

The molybdenum phosphate building block in **1** and **2** is the $[Mo_6O_{15}(HPO_4)(H_2PO_4)_3]^{5-}$ unit (**3**), which has been previously observed in two sodium molybdenum phosphates[8,11] and a layered zinc molybdenum phosphate.[22] This cluster consists of three metal–metal-bonded, oxo-bridged Mo dimers connected together by additional oxo groups into a ring containing six Mo atoms and four phosphate groups, as shown in Figure 1. Three of the four phosphate groups are located on the periphery of the Mo_6 ring and bridge the three nonbonded Mo–Mo contacts, and each have two terminal P–OH groups. The remaining PO_4 group has three

(14) Mundi, L. A.; Haushalter, R. C. *Inorg. Chem.* **1990**, *29*, 2879.
(15) Tsai, M.; Feng, S.; Greenblatt, M.; Haushalter, R. C. *Solid State Ionics*, in press.
(16) Corcoran, E. W., Jr. *Inorg. Chem.* **1990**, *29*, 157.
(17) Haushalter, R. C.; Strohmaier, K. G.; Lai, F. W. *Science (Washington, D.C.)* **1989**, *246*, 1289.
(18) Mundi, L. A.; Strohmaier, K. G.; Goshorn, D. P.; Haushalter, R. C. *J. Am. Chem. Soc.* **1990**, *112*, 8182.
(19) King, H. E., Jr.; Mundi, L. A.; Strohmaier, K. G.; Haushalter, R. C. *J. Solid State Chem.* **1991**, *92*, 1.
(20) Haushalter, R. C.; Mundi, L. A.; Strohmaier, K. G.; King, H. E., Jr. *J. Solid State Chem.* **1991**, *92*, 154.
(21) Haushalter, R. C.; Mundi, L. A.; Strohmaier, K. G. *Inorg. Chem.* **1991**, *30*, 153.
(22) Haushalter, R. C.; Mundi, L. A. *Inorg. Chem.* **1992**, *31*, 3050.

Table II. Positional Parameters and B_{eq}[a] Values (Å^2) for **1** and **2**

atom	x	y	z	B_{eq}	atom	x	y	z	B_{eq}
				Complex **1**					
Mo(1)	0.4612(2)	0.6694(2)	0.1820(2)	3.2(4)	O(6)	0.317(1)	0.758(2)	0.3166	3(2)
Fe(1)	1/2	1/2	1/2	2.791(4)	O(7)	0.520(1)	0.782(1)	0.074(1)	5(4)
Fe(2)	0	1.000	0	2.320(4)	O(8)	0.102(1)	0.886(3)	0.1019	8(4)
P(1)	0.1824(5)	0.765(1)	0.1824	5(1)	O(9)	0.3552(7)	0.3552	0.3552	5.13(2)
P(2)	0.3950(3)	0.3950	0.3950	3.057(5)	N(1)	0.144(1)	0.1443	0.1443	4(1)
O(1)	0.555(1)	0.5553	0.301(2)	3(2)	N(2)	0.450(2)	0.076(3)	0.4501	8(1)
O(2)	0.320(1)	0.759(1)	0.116(1)	5(3)	N(3)	0.859(1)	0.460(2)	0.8594	3.1(5)
O(3)	0.196(2)	0.636(3)	0.1961	9(5)	N(4)	0.714(2)	0.7138	0.7138	3(1)
O(4)	0.551(1)	0.5507	0.101(2)	4(3)	C(1)	0.187(1)	0.1874	0.1874	4(1)
O(5)	0.345(1)	0.543(2)	0.3453	3(2)	C(2)	0.065(2)	0.0648	0.272(4)	6.2(9)
				Complex **2**					
Mo(1)	−0.2420(2)	0.6742(2)	0.0422(2)	0.89(7)	O(18)	0.292(1)	0.604(1)	0.193(1)	0.8(3)
Mo(2)	−0.2330(2)	0.6799(2)	−0.1548(2)	0.78(7)	O(19)	0.370(1)	0.795(1)	0.209(2)	1.1(3)
Mo(3)	0.0463(2)	0.6930(2)	−0.1457(2)	0.92(7)	O(20)	0.147(1)	0.754(1)	0.173(1)	0.9(3)
Mo(4)	0.2435(2)	0.6828(2)	0.0598(2)	0.79(7)	O(21)	0.309(2)	0.604(1)	0.421(2)	1.6(3)
Mo(5)	0.2304(2)	0.6698(2)	0.3234(2)	0.72(7)	O(22)	0.366(1)	0.783(1)	0.404(1)	1.0(3)
Mo(6)	0.0237(2)	0.6663(2)	0.3168(2)	0.94(7)	O(23)	0.543(2)	0.859(1)	0.431(2)	1.8(4)
Fe(1)	0.3133(3)	1.0560(2)	0.4908(3)	0.5(1)	O(24)	0.351(2)	0.953(1)	0.368(2)	1.5(3)
Fe(2)	0	1/2	0	0.6(2)	O(25)	0.384(2)	0.974(2)	0.613(2)	2.9(4)
P(1)	0.0190(6)	0.7968(5)	0.1239(6)	0.9(2)	O(26)	0.155(1)	0.773(1)	0.408(2)	1.0(3)
P(2)	−0.1585(6)	0.8536(5)	−0.2402(6)	1.0(2)	O(27)	0.056(2)	0.600(1)	0.413(2)	1.6(3)
P(3)	0.4056(6)	0.8478(5)	0.3524(6)	1.1(2)	O(28)	0.152(2)	0.963(1)	0.421(2)	1.9(4)
P(4)	−0.1829(6)	0.8333(5)	0.3300(7)	1.5(2)	O(29)	0.023(1)	0.913(1)	0.717(2)	1.1(3)
Na(1)	0.434(1)	0.9436(7)	0.007(1)	1.8(4)	O(30)	−0.071(2)	0.771(1)	0.390(2)	1.8(3)
Na(2)	−0.159(2)	0.972(2)	0.178(2)	1.0(4)	O(31)	−0.258(2)	0.786(1)	0.186(2)	1.7(3)
Na(2A)	−0.048(1)	0.990(1)	0.275(1)	1.0(3)	O(32)	−0.260(2)	0.846(1)	0.393(2)	1.6(3)
O(1)	−0.377(2)	0.613(1)	−0.030(2)	1.7(3)	O(33)	−0.135(2)	0.942(1)	0.355(2)	2.5(4)
O(2)	−0.273(2)	0.783(1)	−0.035(2)	1.8(3)	O(34)	−0.066(2)	1.151(2)	0.343(3)	5.7(6)
O(3)	−0.149(1)	0.596(1)	0.176(1)	0.6(3)	O(35)	−0.213(4)	1.033(4)	0.040(5)	5(1)
O(4)	−0.953(1)	0.752(1)	0.170(1)	0.9(3)	O(36)	0.374(6)	1.000(5)	0.162(6)	8(1)
O(5)	−0.163(1)	0.586(1)	−0.053(1)	0.7(3)	O(37)	0.461(7)	1.089(6)	0.095(7)	10(2)
O(6)	−0.362(2)	0.618(1)	−0.270(2)	1.8(4)	O(38)	0.366(5)	1.014(4)	−0.144(5)	7(1)
O(7)	−0.126(1)	0.612(1)	−0.239(2)	1.1(3)	O(39)	0.323(7)	0.815(6)	−0.187(7)	11(2)
O(8)	−0.045(2)	0.795(1)	−0.226(2)	1.7(3)	O(40)	0.499(3)	0.847(3)	0.115(3)	9.5(9)
O(9)	−0.046(1)	0.757(1)	−0.025(1)	0.9(3)	O(41)	−0.484(6)	0.321(6)	−0.287(6)	1(1)
O(10)	−0.247(1)	0.796(1)	−0.230(1)	1.0(3)	O(42)	−0.70(1)	0.317(9)	0.51(1)	6(2)
O(11)	−0.216(2)	0.874(1)	−0.368(2)	1.7(3)	O(43)	−0.459(5)	1.221(5)	0.321(6)	5(1)
O(12)	−0.126(2)	0.958(1)	−0.131(2)	2.3(4)	O(44)	−0.511(4)	1.189(4)	0.342(5)	5(1)
O(13)	0.089(1)	0.624(1)	−0.257(2)	1.2(3)	N(1)	0.333(2)	0.445(2)	−0.357(2)	1.6(4)
O(14)	0.172(2)	0.788(1)	−0.019(2)	1.5(3)	C(1)	0.390(2)	0.407(2)	−0.245(3)	1.9(5)
O(15)	0.096(1)	0.592(1)	−0.043(1)	0.7(3)	C(2)	0.401(3)	0.409(2)	−0.436(3)	3.5(7)
O(16)	0.083(1)	0.579(1)	0.196(2)	0.9(3)	C(3)	0.342(3)	0.555(2)	−0.310(3)	2.9(6)
O(17)	0.332(1)	0.624(1)	−0.003(2)	1.6(3)	C(4)	0.209(3)	0.402(3)	−0.438(3)	3.8(7)

[a] $B_{eq} = (8\pi^2/3)[U_{11}(aa^*) + U_{22}(bb^*) + U_{33}(cc^*) + 2U_{12}aa^*bb^* \cos\alpha + 2U_{13}aa^*c^* \cos\beta + 2U_{23}bb^*cc^* \cos\alpha]$.

O atoms that bridge the three nonbonded Mo atoms from the "inside" of the Mo_6 ring and has one terminal P–OH group with the P–O vector normal to the plane defined by the six Mo atoms. Since all the molybdenums have a 5+ charge, this cluster has a 5− charge when the phosphate groups are fully protonated. Hexamers resembling **3**, with a central M atom connecting two $[Mo_6O_{15}(HPO_4)(H_2PO_4)_3]^{5-}$ rings, have been found in all of our molybdenum phosphate preparations in which there is a metal cation present and, conversely, have never been found in the molybdenum phosphate syntheses in which there are no cations present. In both **1** and **2**, the hexamers **3** are found dimerized about an octahedral central Fe atom, to give the $Fe[Mo_6O_{15}(HPO_4)(H_2PO_4)_3]_2$ ($\equiv Fe[Mo_6P_4]_2$) units (**4**), as shown in Figure 2. These dimers have approximate or rigorous $\bar{3}$ symmetry in **1** and **2**. The structures of both **1** and **2** are built up from these $Fe[Mo_6O_{15}(HPO_4)(H_2PO_4)_3]_2$ units bridged together, via their phosphate groups, by additional Fe^{3+}. This generates a three-dimensional lattice whose pores are filled with a mixture of water solvate and the templating cations.

The determination of the structure of phosphate **1**, $(TMA)_2(NH_4)_2[Fe_2Mo_{12}O_{30}(H_2PO_4)_6(HPO_4)_2]\cdot nH_2O$, was not entirely straightforward. When the diffraction patterns of several initial batches of **1** were studied, the results showed that the crystals displayed unit cell parameters that were definitely metrically trigonal or hexagonal. However, comparison of the intensity of reflections that should have been equivalent under hexagonal symmetry gave ambiguous results. The R factors for merging of the supposedly equivalent reflections were in the 15–20% range, indicating the symmetry was nearly hexagonal. When data sets collected on these crystals were solved, the heavy-atom positions were readily found and made chemical sense but the refinements would not converge to acceptably low values. A crystal was finally examined that displayed a reasonable intensity distribution corresponding to hexagonal symmetry. The data were collected and solved in a C-centered monoclinic setting but was successfully transformed to a hexagonal cell. Solution of these data converged to give very reasonable bond distances and angles, but the R factors remained rather high, near 9%. The isotropic thermal parameters for this structural solution of **1** had values that were uniformly about 3 times higher than the typical values we have found for a large number of our 3-D molybdenum phosphate structures. One possible explanation for the high R factors and large thermal parameters is that the symmetry of the crystals is actually lower than hexagonal and the atomic positions deviate slightly from those corresponding to true hexagonal symmetry. There were no intense superstructure reflections indicative of a larger cell. A possible explanation for a lowering of the symmetry is suggested below.

The structure of **1** will be discussed by progressing from the gross structural connectivities to local-bonding patterns. The asymmetric unit and the atom-numbering scheme for **1** are shown in Figure 3. The structure consists of the $Fe(1)[Mo_6O_{15}(H_2-$

Table III. Selected Interatomic Distances (Å) for **1** and **2**

		Complex **1**	
Mo(1)–Mo(1)	2.589(4)	Mo(1)–O(6)	2.095(9)
Mo(1)–O(1)	2.01(1)	Mo(1)–O(7)	1.63(2)
Mo(1)–O(2)	2.06(1)	Fe(1)–O(1)	2.13(2) (×8)
Mo(1)–O(4)	1.94(1)	Fe(2)–O(8)	1.91(2) (×8)
Mo(1)–O(5)	2.27(1)		
		Complex **2**	
Mo(1)–Mo(2)	2.587(3)	Mo(6)–O(16)	2.02(2)
Mo(1)–O(1)	1.67(2)	Mo(6)–O(26)	1.96(2)
Mo(1)–O(2)	1.96(2)	Mo(6)–O(27)	1.63(2)
Mo(1)–O(3)	2.10(2)	Mo(6)–O(30)	2.06(2)
Mo(1)–O(4)	2.28(2)	Fe(1)–O(11)	1.93(2)
Mo(1)–O(5)	1.97(1)	Fe(1)–O(23)	1.91(2)
Mo(1)–O(31)	2.05(2)	Fe(1)–O(24)	1.95(2)
Mo(2)–O(2)	1.94(2)	Fe(1)–O(25)	2.01(2)
Mo(2)–O(5)	1.97(2)	Fe(1)–O(28)	2.17(2)
Mo(2)–O(6)	1.65(2)	Fe(1)–O(32)	1.98(2)
Mo(2)–O(7)	2.09(2)	Fe(2)–O(5)	2.18(1)
Mo(2)–O(9)	2.26(2)	Fe(2)–O(5)	2.18(1)
Mo(2)–O(10)	2.08(2)	Fe(2)–O(15)	2.21(1)
Mo(3)–Mo(4)	2.592(3)	Fe(2)–O(15)	2.21(1)
Mo(3)–O(7)	2.09(2)	Fe(2)–O(16)	2.10(2)
Mo(3)–O(8)	2.07(2)	Fe(2)–O(16)	2.10(2)
Mo(3)–O(9)	2.28(2)	Na(1)–O(35)	2.57(5)
Mo(3)–O(13)	1.69(2)	Na(1)–O(36)	2.31(6)
Mo(3)–O(14)	1.93(2)	Na(1)–O(37)	1.92(7)
Mo(3)–O(15)	1.95(2)	Na(1)–O(37)	2.20(7)
Mo(4)–O(14)	1.93(2)	Na(1)–O(38)	2.19(6)
Mo(4)–O(15)	1.96(2)	Na(1)–O(38)	2.28(6)
Mo(4)–O(17)	1.67(2)	Na(1)–O(39)	2.35(8)
Mo(4)–O(18)	2.12(2)	Na(1)–O(40)	2.05(4)
Mo(4)–O(19)	2.06(2)	Na(2)–Na(2A)	1.32(3)
Mo(4)–O(20)	2.25(2)	Na(2)–O(29)	2.39(3)
Mo(5)–Mo(6)	2.594(3)	Na(2)–O(33)	2.29(3)
Mo(5)–O(16)	1.98(2)	Na(2)–O(34)	2.59(3)
Mo(5)–O(18)	2.08(2)	Na(2)–O(35)	1.98(5)
Mo(5)–O(20)	2.31(2)	Na(2)–O(38)	2.45(6)
Mo(5)–O(21)	1.64(2)	Na(2A)–O(28)	2.38(2)
Mo(5)–O(22)	2.07(2)	Na(2A)–O(29)	1.92(2)
Mo(5)–O(26)	1.94(2)	Na(2A)–O(33)	2.10(2)
Mo(6)–O(3)	2.12(1)	Na(2A)–O(34)	2.13(3)
Mo(6)–O(4)	2.29(2)		

$PO_4)_3(HPO_4)]_2 \equiv Fe[Mo_6P_4]_2$ dimers (**4**) bonded through some of their phosphate O atoms to additional octahedrally coordinated Fe(2). Each $Fe[Mo_6P_4]_2$ unit contacts six different, but crystallographically identical, Fe(2) atoms (Figure 2), while each octahedral Fe(2) is bonded to one of the phosphate O atoms from six independent $Fe[Mo_6P_4]_2$ units. Both $Fe[Mo_6P_4]_2$ and Fe(2) are centered on sites with $\bar{3}$ symmetry. The Mo_6 rings lie in planes perpendicular to [0001].

One can think of the connectivity of the Fe(2) and $Fe[Mo_6P_4]_2$ moieties as follows. Consider the six terminal O atoms of each $Fe[Mo_6P_4]_2$ unit, which are coordinated to the six Fe(2) atoms, to lie at the vertices of a trigonally distorted octahedron, oct_{dist}. The structure can then be considered to be built up from the oct_{dist} sharing its corners with the octahedral Fe(2), $oct_{Fe(2)}$. Thus each oct_{dist} shares its six vertices with six different $oct_{Fe(2)}$ atoms and vice versa. As a final conceptual simplication, if one now considers oct_{dist} and $oct_{Fe(2)}$ to be identical octahedra, their connectivity is simply that of the octahedra in the ReO_3 structure type ($Pm\bar{3}m$) where the hexagonal *c* axis corresponds to one of the ⟨111⟩ directions in the cubic ReO_3 lattice.

The connectivity of the $Fe[Mo_6P_4]_2$ units and Fe(2) is shown in Figure 4, which is a view perpendicular to [0001] and is approximately along the *x* direction. There are three of the $Fe[Mo_6P_4]_2$ dimers per repeat along the *c* axis, giving an *..abcabc..* stacking sequence in this direction for the $Fe[Mo_6P_4]_2$ units. In Figure 5, parts a, b, and c show projections containing the cell contents approximately from the sections $0–{}^1/_3$, ${}^1/_3–{}^2/_3$, and ${}^2/_3–1$, respectively, along [0001]. Again referring to Figure 5, it is easy to see that the centers of the $Fe[Mo_6P_4]_2$ units correspond exactly to the location of the sphere centers in cubic closest packed spheres, exactly as one would expect from the analogy to the ReO_3 structures type discussed above. Likewise, the Fe(2) atoms also occupy positions that are topologically identical to the spheres in cubic closest packed spheres.

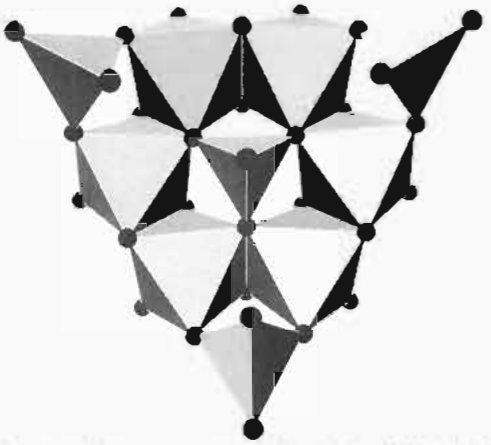

Figure 1. Polyhedral representation of the $Mo_6O_{15}(HPO_4)(H_2PO_4)_3]^{5-}$ unit. The ring of edge-sharing MoO_6 octahedra contains alternating bonding (ca. 2.6 Å) and nonbonding (ca. 3.5 Å) Mo···Mo contacts.

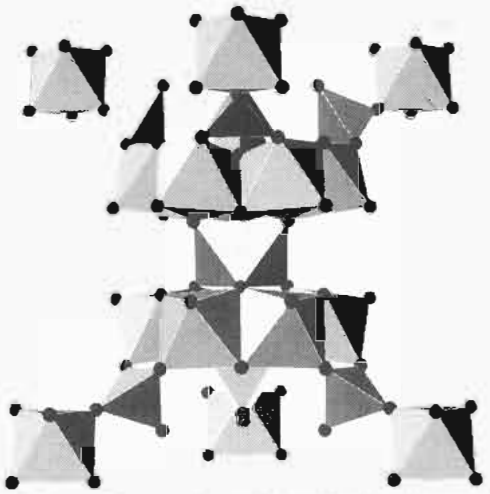

Figure 2. Polyhedral representation of the $Fe[Mo_6O_{15}(HPO_4)(H_2PO_4)_3]_2$ ($\equiv Fe[Mo_6P_4]_2$) (**4**) units present in **1**. Also shown are the six $Fe_{6/6}$ octahedra bonded to the six exo P–OH groups on the periphery of the two Mo_6P_4 rings. A similar unit is present in **2** but without all of the terminal P–OH groups protonated.

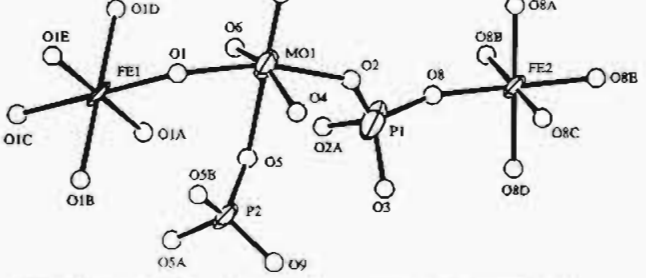

Figure 3. Asymmetric unit and atom-numbering scheme for **1**.

There are two terminal P–O groups on the three PO_4 tetrahedra that reside on the periphery of each Mo_6 ring and one terminal P–O on the central PO_4 tetrahedron. As shown in the picture of dimer **4** in Figure 2, the two terminal P–O groups on each of three peripheral PO_4 groups can be considered as endo and exo with respect to the central P–O. The three exo P–OH groups on the periphery are coordinated to three different Fe(2) octahedra.

The remaining three endo P–OH groups, as well as the central terminal P–OH, are not coordinated to iron. As shown in Figure

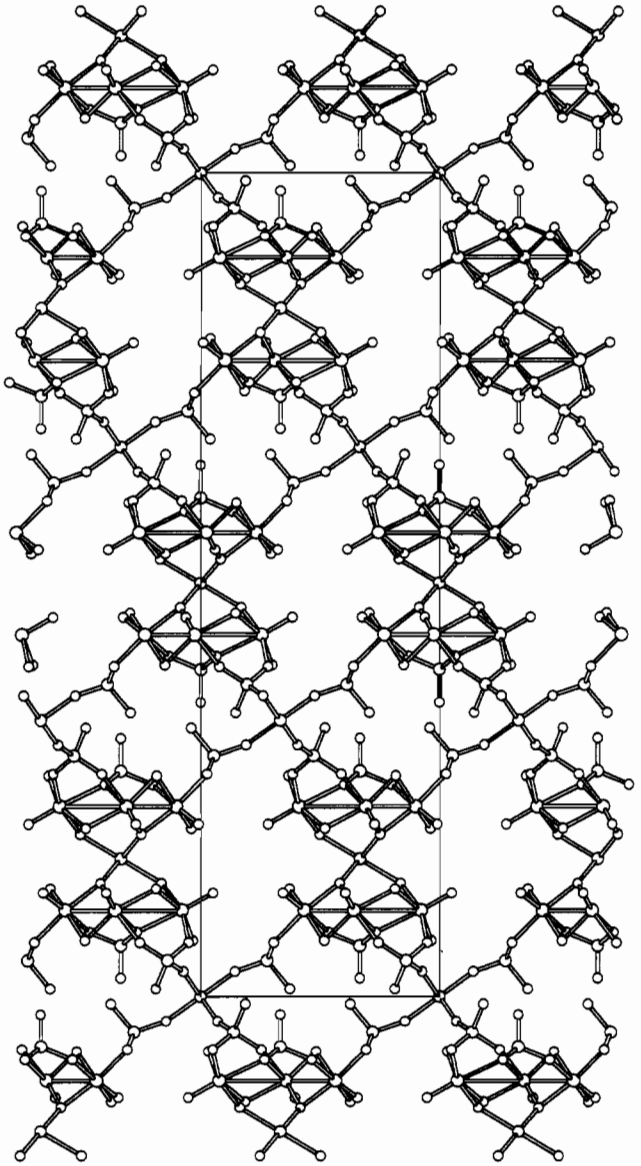

Figure 4. View of the structure of **1** (hexagonal setting of unit cell) along *x* illustrating the *..abc..* stacking sequence for the $Fe[Mo_6P_4]_2$ units along [0001]. Note the "layers" of O atoms, parallel to (001), with the Mo, P, and Fe cations between the "layers".

6a, the O atoms of the three endo P–OH groups are all equidistant from the O atom of the central phosphate at 3.19(2) Å, as required by the hexagonal symmetry. With only very small movements, the endo P–OH is within hydrogen-bonding distance of the central P–OH. Since there are only two unshared pairs of electrons on the O atom of the central P–OH group, it is not possible for all three of the endo P–OH groups to hydrogen bond to it in a symmetrical fashion. This would have to induce a distortion of the structure due to the pairwise alternation of long and short O···O contacts around the ring arising from the H-bonds. This is illustrated schematically in Figure 6b–d. This pairing of the H-bonds is not compatible with the $\bar{3}$ symmetry required of the $Fe[Mo_6P_4]$ units in $R\bar{3}m$ on a local level, but is compatible if averaged out over the entire structure. Note that this distortion would be expected to affect the entire structure as the exo O atom of the PO_4 group, which would likely occupy a slightly different position depending on whether the endo O was H-bonded to the central P–OH, acts a bridge between the Fe(2) and the $Fe[Mo_6P_4]_2$ dimers. The net overall effect would therefore be slightly different positions for the atoms in each $Fe[Mo_6P_4]_2$. If all orientations of this hydrogen-bonding pattern were present in equal amounts, the compound would display rhombohedral symmetry and the rather small positional variations would be reflected in the higher

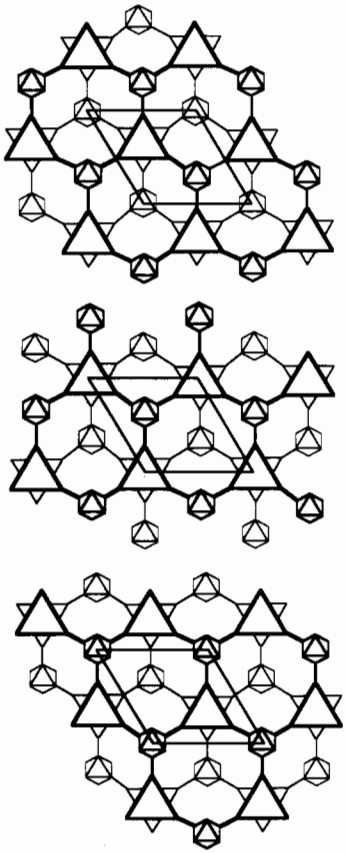

Figure 5. Schematic illustration of how the $Fe[Mo_6P_4]_2$ units are bonded together to form the lattice of **1**. Parts a, b, and c (top, middle, and bottom) show projections containing the cell contents approximately from the sections $0–{}^1/_3$, ${}^1/_3–{}^2/_3$, and ${}^2/_3–1$, respectively, along *c*. The triangles represent the $[Mo_6O_{15}(H_2PO_4)_3(HPO_4)]$ units, while the octahedra (viewed down their 3-fold axes) represent the Fe(2) atoms.

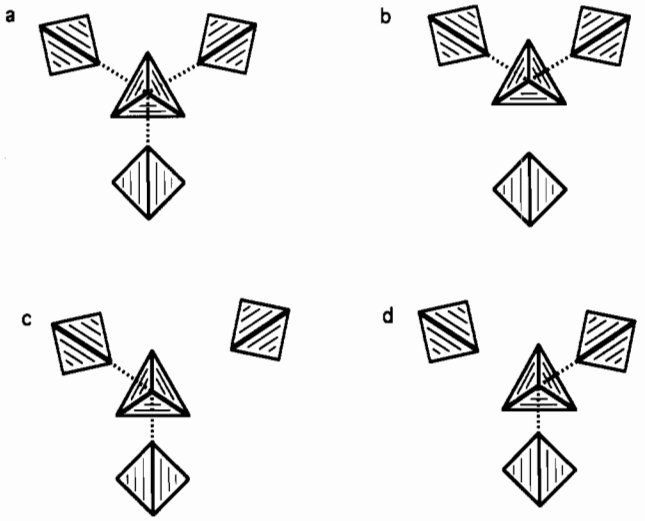

Figure 6. Schematic representation of possible hydrogen-bonding patterns between the central P–OH and the endo P–OH: (a) pattern that conforms to the symmetry of $R\bar{3}m$ with all three H-bonds of equal length; (b–d) central P–OH H-bonding to only two of the three endo P–OH groups at any one time. None of the patterns b–d are compatible with $R\bar{3}m$ symmetry.

than usual thermal parameters found in the crystal structure. However, any correlation in the hydrogen-bonding patterns in neighboring $Fe[Mo_6P_4]_2$ units could provide a possible explanation for the deviations from hexagonal symmetry observed in the intensities of the Bragg reflections from some samples of **1**. Qualitative support for this idea comes from the fact that the isotropic thermal parameters for the symmetry-equivalent peripheral phosphate groups are noticeably larger than those for

the central phosphate. The B_{eq} value for the P atom of the peripheral PO_4 is 60% larger than that of the central P while the endo and exo O atom thermal parameters are over twice as large as the average for the other O atoms in the structure. Thus, the intracluster asymmetric H-bonding pattern could provide an explanation for both the large thermal parameters and the slight deviations from pure rhombohedral symmetry sometimes observed for **1**.

The anionic ferric molybdenum phosphate framework in phosphate **1**, $(TMA)_2(NH_4)_2[Fe_2Mo_{12}O_{30}(H_2PO_4)_6(HPO_4)_2]\cdot nH_2O$, has a charge of 4– per formula unit which is balanced by a mixture of TMA^+ and NH_4^+ cations. The amount of NH_4^+ and H_2O in **1** was determined as follows. Assuming all of the terminal P–OH groups are protonated and the irons have a 3+ charge, $[Fe_2Mo_{12}O_{30}(H_2PO_4)_6(HPO_4)_2]$ requires a 4– charge. This charge is compensated by two TMA^+ and two NH_4^+ cations, which is consistent with the N content from elemental analysis (% N: calcd 1.94; found 1.90, 1.98). In the crystal structure determination, it was not possible to differentiate the ammonium cations from the water of solvation. Not surprisingly, in light of the high standard deviations found for the positional and thermal parameters, the quality of the refinement and the thermal parameters of these atoms were relatively insensitive to whether they were considered to be N or O.

The other charge-compensating cations within the pores of **1** are the TMA^+. As found in several of our other structurally characterized molybdenum phosphates,[9] there appears to be a segregation of the overall structure into regions of hydrophobic and hydrophilic interactions. The nonpolar tetraalkylammonium cations are in close proximity to the molybdenyl groups, while the polar water molecules and ammonium cations are near the P–OH groups. This is also the case for **2**, as discussed below.

The thermal gravimetric analysis (TGA) of **1** showed an approximately 5% weight loss, mostly below 100 °C, corresponding to the removal of loosely held water in the micropores of **1**. To investigate the amount and mobility of the water solvate within the pores of **1**, if the low-temperature weight loss observed in the TGA corresponded to water that could be absorbed/desorbed reversibly from the internal pores of the crystal, the water absorption isotherms were measured.

The water absorption isotherm experiments measure the weight change of the sample as a function of the water vapor pressure at constant temperature. The initial absorption isotherm gives information regarding the amount of guest molecules absorbed, the shape of the curve tells if the guests are being sorbed into internal micropores, and the desorption isotherm data show if the absorption is reversible.[23] The water absorption and desorption isotherms for **1** are shown in Figure 7. The sample was first outgassed at $<10^{-3}$ Torr and 150 °C for 1 h. It was then exposed to increasing water vapor pressure and the weight change recorded. The water vapor pressure was then decreased and the weight loss measured. The results indicate a Brunauer type I absorption isotherm[23] indicative of the filling of micropores. Figure 7 also shows that there is only a small amount of hysteresis in the sorption/desorption loop, indicating that the absorption and desorption of the water are quite reversible. The amount of water absorbed is between 5 and 6%, consistent with the weight loss assigned to water leaving the solid in the TGA experiment.

One can also infer the internal void volume of a solid from absorption isotherms. If one assumes that the density of the absorbed water is equal to 1 $g\cdot cm^{-3}$, then the volume of the sorbed water (i.e. the void space the water is filling) is just equal to the weight percent water absorbed multiplied by the density of the absorber. In the case of **1**, the density is calculated to be 2.84 $g\cdot cm^{-3}$ from the X-ray data, so the water is filling about 17 vol % of the solid based on an uptake of 6 wt % water. This is in

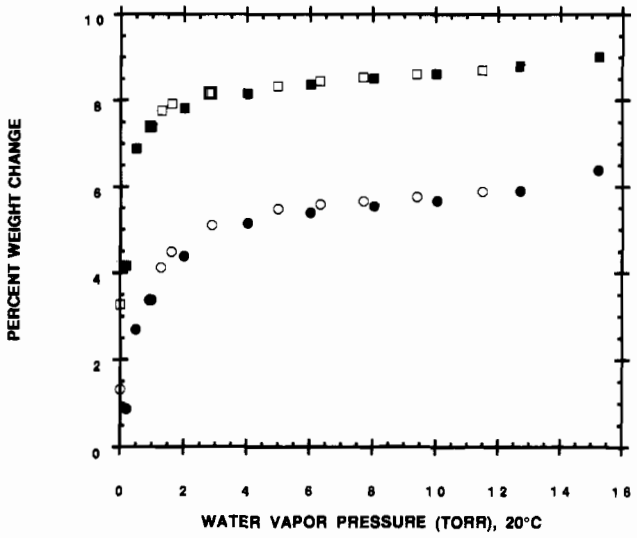

Figure 7. Water absorption isotherms for **1** (circles) and **2** (squares) at 20 °C. The fillted symbols are the absorption and the open ones the desorption data.

reasonable agreement with a value of 6.8 wt % water calculated from the X-ray data. This weight of reversibly sorbed water corresponds to an n of about 11 in the formula $(TMA)_2(NH_4)_2[Fe_2Mo_{12}O_{30}(H_2PO_4)_6(HPO_4)_2]\cdot nH_2O$. Note that this is the volume absorbed with TMA cations still present. As a rough approximation, the 10 atoms in the two TMA^+ cations have a volume approximately equal to the 11 water solvates. Therefore the internal void volume in the micropores of **1** occupied by both cations and solvate is approximately 30 vol %.

The thermal behavior of the cations was also investigated with TGA. In the 200–350 °C range, there is a weight loss possibly due to the loss of NH_3 from the NH_4^+ cations. Then there is a large weight loss in the 350–500 °C range, centered at about 410 °C, corresponding to the thermal decomposition of the TMA cations.

The other phosphate described in this study, **2**, $(TMA)_2Na_4[Fe_3Mo_{12}O_{30}(H_xPO_4)_8]\cdot nH_2O$, has a very complicated structure whose gross overall features resemble those of phosphate **1**. It is built up from dimeric $Fe[Mo_6P_4]_2$ units similar to those found in **1**. The main difference between the two structures is that in **1** the $Fe[Mo_6P_4]_2$ units are held together by Fe^{3+} centers while in **2** the $Fe[Mo_6P_4]_2$ moieties are bonded together by phosphate-bridged Fe^{3+} dimers. Another difference is that **2** contains Na^+ ions bound to the phosphate groups as discussed below. These differences completely remove the high symmetry found in **1**, and phosphate **2** crystallizes in the triclinic space group $P\bar{1}$.

Phosphates **1** and **2** are synthesized under quite similar reaction conditions. The reactions of Na_2MoO_4, Mo, $FeCl_3$ (TMA)OH, H_3PO_4, and H_2O in mole ratios of 5:1:1:2:7:16:150 and 5:1:1:8:18:250 are used for the syntheses of **1** and **2**, respectively, with the further addition of 2 mol equiv of NH_4^+ for **1**. Apparently, the presence of this rather small amount of ammonium cation significantly alters the course of the reaction.

The structure of **2** was routinely solved and refined in $P\bar{1}$. The numbering scheme for the atoms in the asymmetric unit is shown in Figure 8. The broad similarities of **1** and **2** with respect to the overall packing of the $Fe[Mo_6P_4]_2$ clusters are evident in the projection of the structure of **2** down b, the direction that corresponded to [0001] in **1**. Note that the β angle of 119.22(3)° is nearly identical to the corresponding $\gamma = 120°$ in hexagonal **1**. There are tunnels running parallel to all three of the cell edges in **2**. These particular tunnels criss-cross the space between the $Fe[Mo_6P_4]_2$ clusters in several directions.

The main difference between the structures of **1** and **2** lies in the hydrophilic region in the vicinity of the phosphate groups. In **1**, this region contains ammonium and ferric cations, while in **2**

(23) Ruthven, D. M. *Principles of Adsorption and Adsorption Processes*; Wiley & Sons: New York, 1984; p 49.

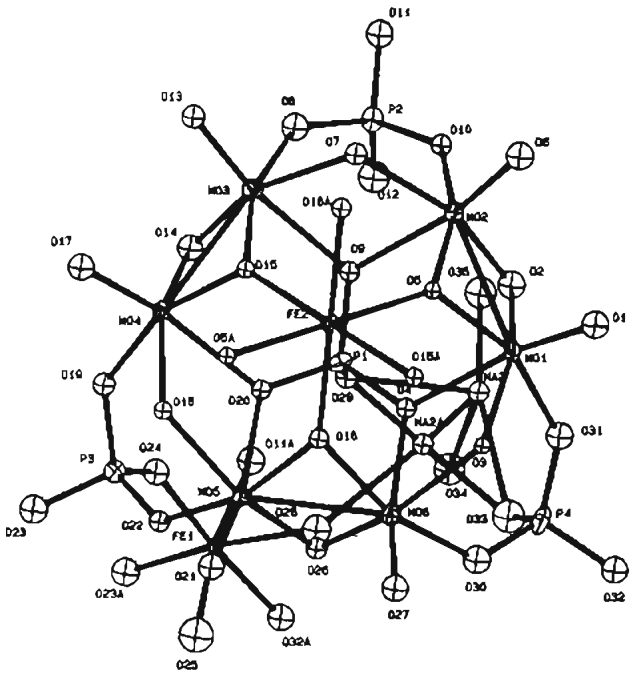

Figure 8. Numbering scheme for the framework atoms in the asymmetric unit of **2**.

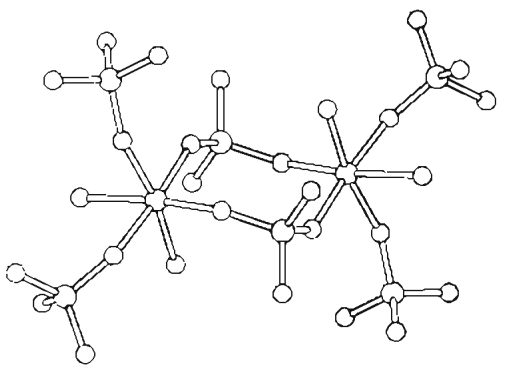

Figure 9. The centrosymmetric ferric dimers. There are two terminal water ligands, one of which is also shared with the $[Na_2(H_2O)_{10}]^{2+}$ cation, on each Fe.

it contains sodium and ferric cations. The extra ferric ions in the framework of **2** as compared to **1** expand the hydrophilic region between the ends of adjacent $Fe[Mo_6P_4]_2$ units and allow the incorporation of hydrated Na^+ cations. The structure of the region enclosed by the phosphate groups in **2** contains phosphate-bridged iron dimers, hydrated sodium ion dimers, monomeric sodium ions, and water molecules. The dimer of the Fe^{3+} cations is contacted by two O atoms from each bridging phosphate and resides on a $\bar{1}$ site; the structure is shown in Figure 9. Each iron contacts four phosphate groups, three of which are crystallographically independent. The two phosphate groups that bridge the ferric ions each share two O atoms with the two irons. The remaining phosphate groups contact the irons with only one O atom each. Each iron center has two terminal water ligands, O(28) and O(25), bonding to Fe at distances of 2.17(2) and 2.01(2) Å, respectively. O(28), with the longer Fe–O distance, is also bound to one of the sodium ions, while the other O atom is not bound to a second metal center but rather is probably hydrogen-bonded to O atoms 44, 36, 43, and 38 at distances of 2.86(5), 2.97(6), 3.00(6), and 3.07(6) Å, respectively. Another interesting cation found in the phosphate region of the structure also lying on a $\bar{1}$ site is $Na_2(H_2O)_{10}^{2+}$, which is shown in Figure 10. The dimer can be roughly described as a pair of face-sharing NaO_6 octahedra with an additional O atom symmetrically inserted into the plane containing the three μ_2-O atoms to give a shared square of μ_2-O atoms. The remaining cation is a mononuclear

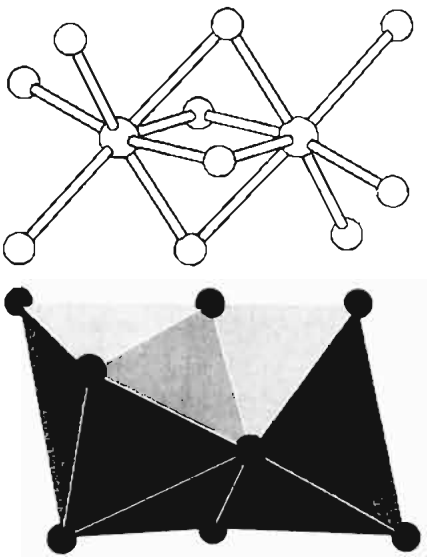

Figure 10. The centrosymmetric $[Na_2(H_2O)_{10}]^{2+}$ cation found in **2** as (a, top) ball-and-stick and (b, bottom) polyhedral representations.

hydrated sodium cation. This mononuclear sodium is disordered between two sites, which are ca. 1 Å apart, in the ratio of 6:4.

The exact disposition of the charges on the atoms in **2** is not quite as unambiguous as in the case of **1**. If the fully protonated Mo_6P_4 units have a 5– charge each and the iron atoms are all Fe^{3+}, then there is a excess of five positive charges per formula unit of $(TMA)_2Na_4[Fe_3Mo_{12}O_{30}(H_xPO_4)_8]\cdot 16H_2O$ if $x = {}^{14}/_8 = 1.75$ as in the case of the fully protonated Mo_6P_4 clusters. The most reasonable assumption to make is that 5 of the 14 terminal P–OH groups in each $Fe[Mo_6P_4]_2$ dimer are unprotonated to give a value of ${}^9/_8 = 1.125$ for x in the formula for **1**.

The TGA of **2** shows an abrupt weight loss between room temperature and ca. 75 °C and an additional broader loss in the 100–225 °C range, which we assign to solvate water and water coordinated to the metal cations, respectively. There is an additional weight loss centered at ca. 425 °C due to the thermal decomposition of the TMA cations. The water absorption isotherm for **2** is shown in Figure 7. After being degassed for 0.5 h at 145 °C, the sample showed about a 9 wt % uptake of water into the micropores. The absorption–desorption loop shows essentially no hysteresis, indicative of a quite reversible process. Using the value for the density of 2.75 g·cm^{-3} obtained from the X-ray data, a value of 25 vol % internal void space filled by the water was calculated.

The total number of nonframework O atoms found in the crystal structure, which correspond to water solvate, was found to be 16 per $(TMA)_2Na_4[Fe_3Mo_{12}O_{30}(H_xPO_4)_8]\cdot nH_2O$ formula unit (i.e. $n = 16$). The weight percent water calculated from this formula, 9.1 wt %, is in excellent agreement with the 9 wt % value found from the water absorption isotherm. About 25% of the total water present is coordinated to iron, and it appears as though it can be reversibly removed.

Conclusions

The high-yield, single-phase synthesis of ferric molybdenum phosphates **1** and **2**, along with our recently reported example of layered $(TMA)_2(H_3O)_2[Zn_3Mo_{12}O_{30}(HPO_4)_2(H_2PO_4)_6]\cdot 11.5H_2O$,[22] illustrates the utility of hydrothermal syntheses in the preparation of structually complex inorganic solids at relatively low temperatures. Like hydrothermal syntheses involving zeolites and aluminum phosphates, the synthesis of the molybdenum phosphates is very sensitive to the nature and amounts of the templating species present.

Both **1** and **2** have very complex structures, with *five* different cationic sites ordered into the oxide framework, which were assembled from very simple, mostly monomeric starting materials.

As with most hydrothermal syntheses, the large number of variables involved with the synthesis of **1** and **2** renders it difficult to assess how the complicated frameworks are formed. The positive aspect of this complexity is that once the role of the templating cation becomes understood, it can be used as a basis for control in assembling large, complicated inorganic structures.

The microporosity of these ferric molybdenum phosphates makes them one of the few examples of a microporous solid with an octahedral–tetrahedral framework. Furthermore, as suggested by the absorption isotherms obtained for **2**, it may be possible to create vacant coordination sites on transition metal sites within the micropores, but this phenomenon awaits structural confirmation. As recently discussed,[7] materials allowing shape-selective access to vacant coordination sites on a transition element within the micropores of a heat-stable oxide framework might prove interesting.

Acknowledgment. We are greatful to Dr. Bev Vincent of the Molecular Structure Corp. for collection and solution of the X-ray data.

Supplementary Material Available: Tables giving crystal data and details of the structure determination, atom coordinates, site occupancies, bond lengths and angles, and anisotropic temperature parameters (32 pages). Ordering information is given on any current masthead page.